Can the $C_5H_5 + C_5H_5 \rightarrow C_{10}H_{10} \rightarrow C_{10}H_9 + H/C_{10}H_8 + H_2$ Reaction Produce Naphthalene? An Ab Initio/RRKM Study

A. M. Mebel* and V. V. Kislov

Department of Chemistry and Biochemistry, Florida International University, Miami, Florida 33199

Received: June 24, 2009; Revised Manuscript Received: July 27, 2009

Ab initio and density functional calculations using a variety of theoretical methods (CASSCF, B3LYP, CASPT2, CCSD(T), and G3(MP2,CC)) have been carried out to unravel the mechanism of unimolecular isomerization and dissociation of 9,10-dihydrofulvalene $C_{10}H_{10}$ (**S0**) formed by barrierless recombination of two cyclopentadienyl radicals. Different reaction pathways on the $C_{10}H_{10}$ potential energy surface (PES) are found to lead to the production of 9-H-fulvalenyl radical + H, 9-H-naphthyl radical (a naphthalene precursor) + H, and naphthalene + H_2. RRKM calculations of thermal rate constants and product branching ratios at the high pressure limit show that at temperatures relevant to combustion the 9-H-fulvalenyl radical formed by a direct H loss from **S0** with endothermicity of 76.3 kcal/mol is expected to be the dominant reaction product. The naphthalene precursor 9,10-dihydronaphthalene (**D3**) can be produced from the initial **S0** adduct by a multistep diradical mechanism involving the formation of a metastable tricyclic diradical intermediate, followed by its three-step opening to a 10-member ring structure, which then undergoes ring contraction producing the naphthalene core structure in **D3**, with the highest barrier on this pathway being 70.3 kcal/mol. **D3** can lose molecular hydrogen producing naphthalene via a barrier of 77.7 kcal/mol relative to the initial adduct. Another possibility is a hydrogen atom elimination in **D3** giving rise to the 9-H-naphthyl radical without exit barrier and with overall endothermicity of 59.2 kcal/mol. The pathway to 9-H-naphthyl appears to be preferable as compared to the direct route to 9-H-fulvalenyl at temperatures below 600 K, but the rate constants at these temperatures are too slow for the reaction to be significant. The naphthalene + H_2 channel is not viable at any temperature. The following reaction sequence is suggested for kinetic models to account for the recombination of two cyclopentadienyl radicals:

$$\text{c-}C_5H_5 + \text{c-}C_5H_5 \rightarrow \text{9,10-dihydrofulvalene} \rightarrow \text{9-H-fulvalenyl} + H(C_{10}H_{10}\text{PES})$$

$$\text{9-H-fulvalenyl} \rightarrow \text{naphthalene} + H/\text{fulvalene} + H(C_{10}H_9\text{PES})$$

We conclude that naphthalene can be produced from the recombination of two cyclopentadienyl radicals and is expected to be a favorable product of this reaction sequence at $T < 1000$ K, but this molecule would be formed through isomerizations and H atom loss on the $C_{10}H_9$ PES (after the initial H elimination from $C_{10}H_{10}$ **S0**) and not in conjunction with molecular hydrogen. The alternative product, fulvalene, can potentially contribute to the growth of cyclopentafused polycyclic aromatic hydrocarbons.

1. Introduction

The cyclopentadienyl radical, c-C_5H_5, is an abundant small radical in combustion flames and its reactions can play an important role in the formation and growth of polycyclic aromatic hydrocarbons (PAH),[1−6] along with the generally accepted hydrogen abstraction acetylene addition (HACA) mechanism.[7] The c-C_5H_5 radicals can be produced in hydrocarbon combustion by eq 1, through pyrolysis of cyclopentadiene,[8] by oxidation of phenyl radicals leading to phenoxy radicals followed by their unimolecular decomposition (eq 2),[9−15] or by addition of propargyl radical C_3H_3 to acetylene (eq 3):[16]

$$\text{c-}C_5H_6 \rightarrow \text{c-}C_5H_5 + H \quad (1)$$

$$C_6H_5 + O_2 \rightarrow C_6H_5O + O \quad C_6H_5O \rightarrow \text{c-}C_5H_5 + CO \quad (2)$$

$$C_3H_3 + C_2H_2 \rightarrow \text{c-}C_5H_5 \quad (3)$$

In its turn, cyclopentadienyl can react with other abundant flame molecules resulting in the formation of aromatic species. For instance, c-C_5H_5 has been shown to be a potential benzene precursor through the $CH_3 + C_5H_5$ reaction.[17] Two consecutive additions of acetylene to cyclopentadienyl (eq 4)[18] or an addition of vinylacetylene to c-C_5H_5 (eq 5) are believed to be potential routes to the formation of indene, the smallest cyclopentafused polycyclic aromatic hydrocarbon (CP-PAH):

* Corresponding author. E-mail: mebela@fiu.edu.

10.1021/jp905931j CCC: $40.75
Published on Web 08/14/2009

$$c\text{-}C_5H_5 + 2C_2H_2 \rightarrow C_9H_9 \rightarrow C_9H_8(\text{indene}) + H \quad (4)$$

$$c\text{-}C_5H_5 + C_4H_4 \rightarrow C_9H_9 \rightarrow C_9H_8(\text{indene}) + H \quad (5)$$

The reactions of cyclopentadienyl with itself and with cyclopentadiene occurring on the $C_{10}H_{10}$ and $C_{10}H_{11}$ potential energy surfaces (PES) represent possible pathways to the smallest PAH molecule, naphthalene $C_{10}H_8$. In this case, naphthalene can be potentially formed bypassing the formation of the first aromatic ring, benzene or phenyl radical. Because the production of the first aromatic ring is often considered as a kinetic bottleneck for the growth of PAH in hydrocarbon combustion, understanding of alternative routes leading to polycyclic aromatic molecules is important for the overall knowledge of the PAH formation mechanism.

The $c\text{-}C_5H_5 + c\text{-}C_5H_5$, and $c\text{-}C_5H_5 + c\text{-}C_5H_6$ reactions initially produce 9,10-dihydrofulvalene $C_{10}H_{10}$ and 8,9,10-trihydrofulvalenyl radical $C_{10}H_{11}$, respectively, related to each other by addition/elimination of H radicals. Under high-temperature combustion conditions the H addition/elimination/abstraction reactions can readily occur, and therefore, to unravel the formation of naphthalene from the two cyclic C_5 compounds, one has to consider the entire family of the $C_{10}H_x$ ($x = 8-11$) PESs. On the $C_{10}H_{11}$ surface, the reaction mechanism starting from the intermolecular addition of $c\text{-}C_5H_5$ to a π bond of $c\text{-}C_5H_6$, followed by rearrangements and CH_3 elimination at the final step producing indene, has been suggested by Wang et al. to explain the high indene yield in cyclopentadiene pyrolysis.[8] Our group has recently reported a more detailed G3(MP2,CC)//B3LYP ab initio/statistical theory investigation of the $C_{10}H_{11}$ PES accessed by the $c\text{-}C_5H_5 + c\text{-}C_5H_6$ reaction, which demonstrated that at temperatures relevant to combustion indene is expected to be the major reaction product (>50%) followed by 1,5-dihydroazulene (25−35%), with all other products giving only minor or negligible yields.[19] On the $C_{10}H_9$ surface, a spiran mechanism leading to naphthalene from the 9-H-fulvalenyl radical, produced by the recombination of two cyclopentadienyl radicals followed by an immediate H loss, has been initially introduced by Melius et al.[1] Later, we studied the rearrangements of 9-H-fulvalenyl more comprehensively at the G3(MP2,CC)//B3LYP level and found naphthalene, fulvalene, and azulene as the reaction products at the high-pressure limit, with relative yields depending on temperature. At lower temperatures ($T <$ 1000 K), naphthalene was predicted to be the major product (>50%), whereas at higher temperatures the naphthalene yield rapidly decreased and the formation of fulvalene (a probable precursor of CP-PAH) became dominant.[20] The $C_{10}H_8$ surface has also been carefully mapped out in our recent study where we considered the naphthalene−azulene rearrangements and their fragmentation pathways.[21]

Meanwhile, the $C_{10}H_{10}$ PES remains unexplored in relation to the $c\text{-}C_5H_5 + c\text{-}C_5H_5$ reaction and its role in the formation of naphthalene or its precursors. Combustion kinetics models often include two possible scenarios for this reaction as[5]

$$c\text{-}C_5H_5 + c\text{-}C_5H_5 \rightarrow C_{10}H_{10} \rightarrow C_{10}H_8(\text{naphthalene}) + H + H \quad (6a)$$

$$c\text{-}C_5H_5 + c\text{-}C_5H_5 \rightarrow C_{10}H_{10} \rightarrow C_{10}H_8(\text{naphthalene}) + H_2 \quad (6b)$$

Moreover, Carpenter suggested[22] a diradical mechanism for the formation of naphthalene + H_2 or 9-H-naphthyl radical + H from the recombination of two cyclopentadienyl radicals (Scheme 1), which involves isomerization of the initial 9,10-dihydrofulvalene adduct to a three-member-ring diradical structure followed by a ring-opening to a 10-member-ring intermediate, ring closure to 9,10-dihydronaphthalene, and completed by H_2 or H elimination from the latter. However, the viability of this mechanism has never been tested by ab initio calculations.

SCHEME 1: Diradical Mechanism of the $c\text{-}C_5H_5 + c\text{-}C_5H_5 \rightarrow C_{10}H_{10} \rightarrow C_{10}H_9 + H/C_{10}H_8 + H_2$ Reaction

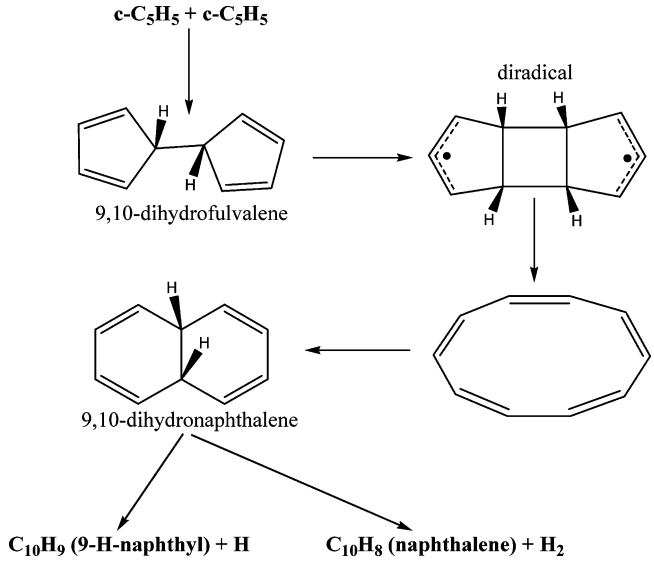

The goal of the present study is to carry out reliable ab initio calculations of the region of the $C_{10}H_{10}$ surface relevant to the reaction of two $c\text{-}C_5H_5$ radicals and the production of naphthalene or its $C_{10}H_9$ precursors via isomerization and dissociation involving diradical (open-shell singlet) $C_{10}H_{10}$ species. These calculations are followed by RRKM calculations of thermal rate constants for unimolecular reactions starting from the initial 9,10-dihydrofulvalene adduct and leading to various reaction products at the high-pressure limit. Finally, the total reaction rate constants and product branching ratios are evaluated at different temperatures relevant to combustion by solving phenomenological first-order kinetic equations using the computed thermal rate constants, with the main goal to assess the feasibility of various rearrangements of 9,10-dihydrofulvalene $C_{10}H_{10}$ leading to naphthalene and other possible products.

2. Computational Methods

Geometries of local minima and transition states were initially optimized using the hybrid density functional B3LYP method[23] with the 6-311G** basis set. However, this method is not expected to be reliable for diradical structures, which may be involved in the reaction mechanism, because of a multireference character of their wave functions. For instance, transition states related to the diradical mechanism shown in Scheme 1 could not be located at the B3LYP level. Therefore, these structures were optimized utilizing the multireference complete active space self-consistent field (CASSCF) approach[24] with the same 6-311G** basis set and the active space containing eight electrons distributed on eight orbitals (8,8). Normally, the calculated occupation numbers for the eight active orbitals ranged between 1.98 and 0.02. A test extension of the active space to (10,10) by adding one extra occupied and one vacant

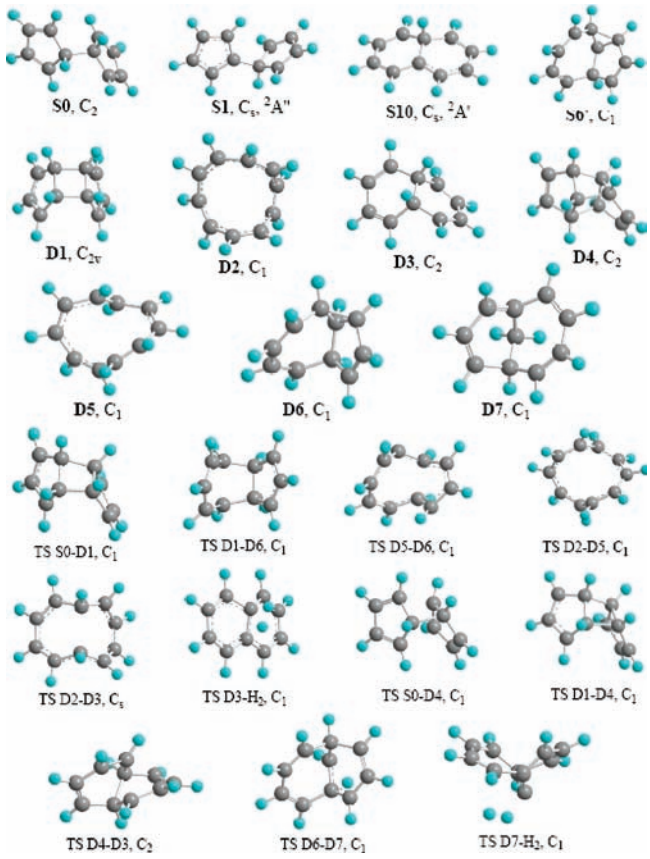

Figure 1. Optimized geometries of $C_{10}H_{10}$ intermediates and transition states and $C_{10}H_9$ products. The structures are calculated at the CASSCF(8,8)/6-311G** level of theory, except for TS D3-H_2, TS D6-D7, **D7**, TS D7-H_2, and **S6′**, for which B3LYP/6-311G** geometries are shown.

orbital gave occupation numbers, respectively, above 1.98 and below 0.02 for the added orbitals, indicating that the (8,8) active space should be sufficient for a proper description of the wave function. For consistency, other $C_{10}H_{10}$ structures were also reoptimized at the CASSCF(8,8)/6-311G** level. All geometry optimizations were run without symmetry constraints, although some optimized structures appeared to be symmetric. Vibrational frequencies were calculated using the same CASSCF(8,8)/6-311G** method and also at B3LYP/6-311G** if the B3LYP geometry optimization was successful, with the goal to characterize the stationary points as local minima or first-order saddle points. Generally, the CASSCF frequencies and molecular structural parameters were utilized to calculate zero-point energy (ZPE) corrections and to perform RRKM computations of reaction rate constants. Calculated Cartesian coordinates of all structures involved in the reactions considered here are collected in Table S1 of Supporting Information along with vibrational frequencies, ZPE corrections, B3LYP and CASSCF total energies, and molecular structural parameters (moments of inertia and rotational constants). Optimized geometries of $C_{10}H_{10}$ local minima and transition states as well as $C_{10}H_9$ products are depicted in Figure 1.

To refine relative energies of $C_{10}H_{10}$ isomers and transition states we applied the multireference second-order perturbation theory CASPT2 method,[25] which takes into account the dynamic correlation effects. The CASPT2 calculations were performed with the same (8,8) active space and 6-311G** basis set. Due to computer limitations, we were not able to include all 50 valence electrons in single and double excitations in CASPT2, that is, in the perturbation theory treatment of the dynamic correlation. A total of 20 valence electrons were instead included in the core at the CASPT2 stage, in addition to 20 actual core electrons. Furthermore, we carried out coupled clusters CCSD(T)/6-311G** calculations and then used the G3(MP2,CC) version[26] of the Gaussian 3 (G3) scheme,[27] where the final energies at 0 K were obtained using the CASSCF or B3LYP (for essentially single-reference reaction products) optimized geometries and ZPE corrections according to the following formula

$$E_0[\mathrm{G3(MP2,CC)}] = E[\mathrm{CCSD(T)/6\text{-}311G(d,p)}] + \Delta E_{\mathrm{MP2}} + \Delta E(\mathrm{SO}) + E(\mathrm{HLC}) + E(\mathrm{ZPE})$$

where $\Delta E_{\mathrm{MP2}} = E[\mathrm{MP2/G3large}] - E[\mathrm{MP2/6\text{-}311G(d,p)}]$ is the basis set correction, $\Delta E(\mathrm{SO})$ is a spin−orbit correction (not included in our calculation), $E(\mathrm{HLC})$ is a higher level correction, and $E(\mathrm{ZPE})$ is the zero-point energy. The relative energies of all species computed at different theoretical levels are collected for comparison in Table 1. The G3-type approach is expected to be chemically accurate for the species with single-reference wave functions; otherwise, the CASPT2 relative energies should be more reliable.

The CASSCF calculations here were performed using the Dalton 2 program package.[28] The B3LYP and MP2 computations were carried out using the Gaussian 98[29] package, whereas the Molpro 2006[30] code was used to calculate spin-restricted (R) CCSD(T) and CASPT2 energies. The RCCSD(T) approach is free of spin contamination and gives correct $\langle \mathbf{S}^2 \rangle$ values of 0.0 and 0.75 for singlet and doublet species, respectively.

First-order thermal rate constants were computed using the conventional canonical Rice-Ramsperger-Kassel-Marcus (RRKM) theory, which is identical to the canonical transition state theory (TST) at the high-pressure limit.[31] The TST calculations are straightforward using the following formula for a unimolecular reaction:

$$k = \sigma \frac{k_{\mathrm{B}}T}{h} e^{-\Delta G_0^{\#}/RT}$$

where R is the Gas constant, k_{B} is the Boltzmann constant, h is the Planck constant, T is the temperature, $\Delta G_0^{\#}$ is the change of the Gibbs free energy from reactants to the transition state, and σ is the reaction path degeneracy. The values of σ used in the calculations are given in Table S2 of Supporting Information. Tunneling corrections (Q_{tun}) to the TST rate constants were computed using the Wigner formula:[31]

$$Q_{\mathrm{tun}} = 1 - \frac{1}{24}\left(\frac{h\upsilon_{\mathrm{s}}}{k_{\mathrm{B}}T}\right)^2\left(1 + \frac{k_{\mathrm{B}}T}{E_0}\right)$$

where υ_{s} is the transition state imaginary frequency and E_0 is the barrier height including ZPE correction.

To calculate rate constants for the H elimination reactions from $C_{10}H_{10}$, which exhibit no exit barriers, we employed the canonical variational transition state theory (CVTST) approach.[32] Within this method, we scanned the minimal energy reaction path (MEP) along the breaking C−H bond and computed 3N−7 vibrational frequencies for all partially optimized MEP structures projecting out the gradient direction. This is achieved by applying the "iop(7/45 = 1)" option in Gaussian 98, which allows to compute 3N−7 frequencies orthogonal to a nonzero gradient at geometric structures that do not represent a stationary

TABLE 1: Relative Energies (kcal/mol) of Various Species Calculated at Different Levels of Theory

		CASPT2		CCSD(T)			
species	B3LYP	CAS[b]	B3LYP[c]	CAS[b]	B3LYP[c]	T1[d]	G3(MP2,CC)[a]
S0,[e] C_2[f]	0.0	0.0	0.0	0.0	0.0	0.010	0.0
S1 + H							76.1[g]
c-C_5H_5 + c-C_5H_5							52.8[g]
TS S0-D1		43.1		43.6		0.017	44.1
D1, C_{2v}[f]	63.3	44.3	45.2	46.7	50.3	0.011	46.1
TS D1-D6		74.1		77.7		0.017	70.3
D6	10.3	18.3	15.6	9.4	8.8	0.010	9.3
TS D5-D6		61.1		60.8		0.018	59.9
D5		32.0		26.3		0.010	25.6
TS D2-D5		65.9		68.6		0.021	66.5
D2	23.4	38.5	36.6	31.5	31.7	0.011	30.1
TS D2-D3, C_s[f]	51.2	66.1	64.8	60.9	61.6	0.012	59.0
D3, C_2[f]	−4.0	0.5	1.8	−3.3	−3.0	0.010	−3.6
TS D3-H_2	70.4		88.8		81.7	0.021	77.7
TS S0-D4	44.6	48.5	39.9	51.1	41.4	0.012	40.9
TS D1-D4		43.7		43.9		0.016	44.5
D4, C_2[f]	18.8	19.3	14.8	8.5	6.8	0.010	9.5
TS D4-D3, C_2[f]	80.0	82.6	80.8	77.7	77.6	0.018	76.3
NP + H_2[g]	−47.5				−35.2		−39.4
S10 + H[g]	50.8				59.2		59.2
TS D6-D7	75.5		80.4		75.9	0.013	74.2
D7	7.5		10.0		5.9	0.012	6.2
TS D7-H_2	103.1		116.9		107.5	0.018	106.0
S6′ + H	90.6				92.2	0.017	93.4
AZ + H_2							−4.3[g]

[a] Between the B3LYP and CASSCF optimized geometries, the geometry giving the lowest CASPT2 and CCSD(T) single-point energy was chosen for G3(MP2,CC) calculations. [b] At the CASSCF optimized geometry. [c] At the B3LYP optimized geometry. [d] The T1 diagnostic value from CCSD/6-311G** calculations. [e] The total energies of **S0** calculated at different theoretical levels are the following (in hartree): B3LYP/6-311G**, −387.097777; CASPT2/6-311G**//CASSCF/6-311G**, −385.223689; CCSD(T)/6-311G**//CASSCF/6-311G**, −386.030448; CASPT2/6-311G**//B3LYP/6-311G**, −385.218075; and CCSD(T)/6-311G**//B3LYP/6-311G**, −386.031086. [f] Symmetry point group is given for $C_{10}H_{10}$ structures only if different from C_1. [g] From ref 20.

point on the PES. These MEP calculations were performed using the unrestricted B3LYP/6-311G** method, and the computed relative energies were then scaled to match the G3(MP2,CC) relative energies of the $C_{10}H_9$ products. According to CVTST,[32] the rate constant for a reaction with no potential energy barrier is found at the point along the MEP where the generalized transition state theory rate constant reaches a minimum. Because the MEP for C−H bond cleavages does not have a distinct saddle point, technically, for each temperature, we calculated a set of conventional TST rate constants $k(T)$ considering each structure on the scanned dissociation path as a transition state candidate and using its molecular structure parameters to compute partition functions. Then, the minimal $k(T)$ value was chosen as the CVTST rate constant at a given temperature, and the respective structure on the MEP represented the variational transition state. All computed rate constants within the 300−3000 K temperature range are collected in Table S2 of Supporting Information. The fourth-order Runge−Kutta method with accuracy monitoring[33] was employed to solve the system of first-order, phenomenological rate equations to obtain relative product yields at different temperatures.

3. Results and Discussion

Reaction Mechanism. The potential energy map for the c-C_5H_5 + c-C_5H_5 → $C_{10}H_{10}$ → $C_{10}H_9$ + H/$C_{10}H_8$ + H_2 reaction with relative energies computed at the G3(MP2,CC) level is illustrated in Figure 2, along with schematic structures of various intermediates (see Figure 1 and Supporting Information for the optimized geometries). The notation of intermediates with a letter "**S**" remained the same as in our previous work on rearrangements of 9-H-fulvalenyl radical formed in the c-C_5H_5 + c-C_5H_5 → **S0** → **S1** + H reaction,[20] whereas the new species are denoted with a letter "**D**". Before going into detail of the reaction mechanism, let us first consider the results for relative energies computed by different theoretical methods (Table 1). The T1 diagnostic values[34] in CCSD calculations are also shown in Table 1. This diagnostic is defined as the Euclidean norm of the t_1 (singles) amplitudes normalized by the number of electrons included in the correlation procedure[34a] and is normally used to distinguish between molecular systems dominated by a single determinant and those requiring a multireference treatment of electron correlation. According to Cramer,[34b] T1 diagnostic values exceeding 0.02 indicate that the use of a multireference method may be needed and that CCSD(T) results should be considered with caution. However, for all calculated structures, the values are rather low, in the range of 0.01−0.02, meaning that the CCSD(T) approach should be able to recover a mild multireference character of the wave functions. One can see that the agreement between the CASPT2 and CCSD(T) energies for all structures is generally close, within 2−3 kcal/mol. Notable exceptions include intermediates **D2**, **D4**, and **D6**, where the differences in relative energies reach 7−10 kcal/mol. Because the T1 diagnostics for these structures are close to 0.01, we expect the CCSD(T) results to be more trustworthy; apparently, the noninclusion of some valence electrons in CASPT2 dynamic correlation treatment causes these deviations. Note also that the use of CASSCF and B3LYP optimized geometries, where both are available, for CASPT2 and CCSD(T) single-point calculations gave close results for the relative energies, with the differences normally in the range of 1−3 kcal/mol. The CASSCF and B3LYP optimized geometries are generally rather similar, with the differences in bond lengths

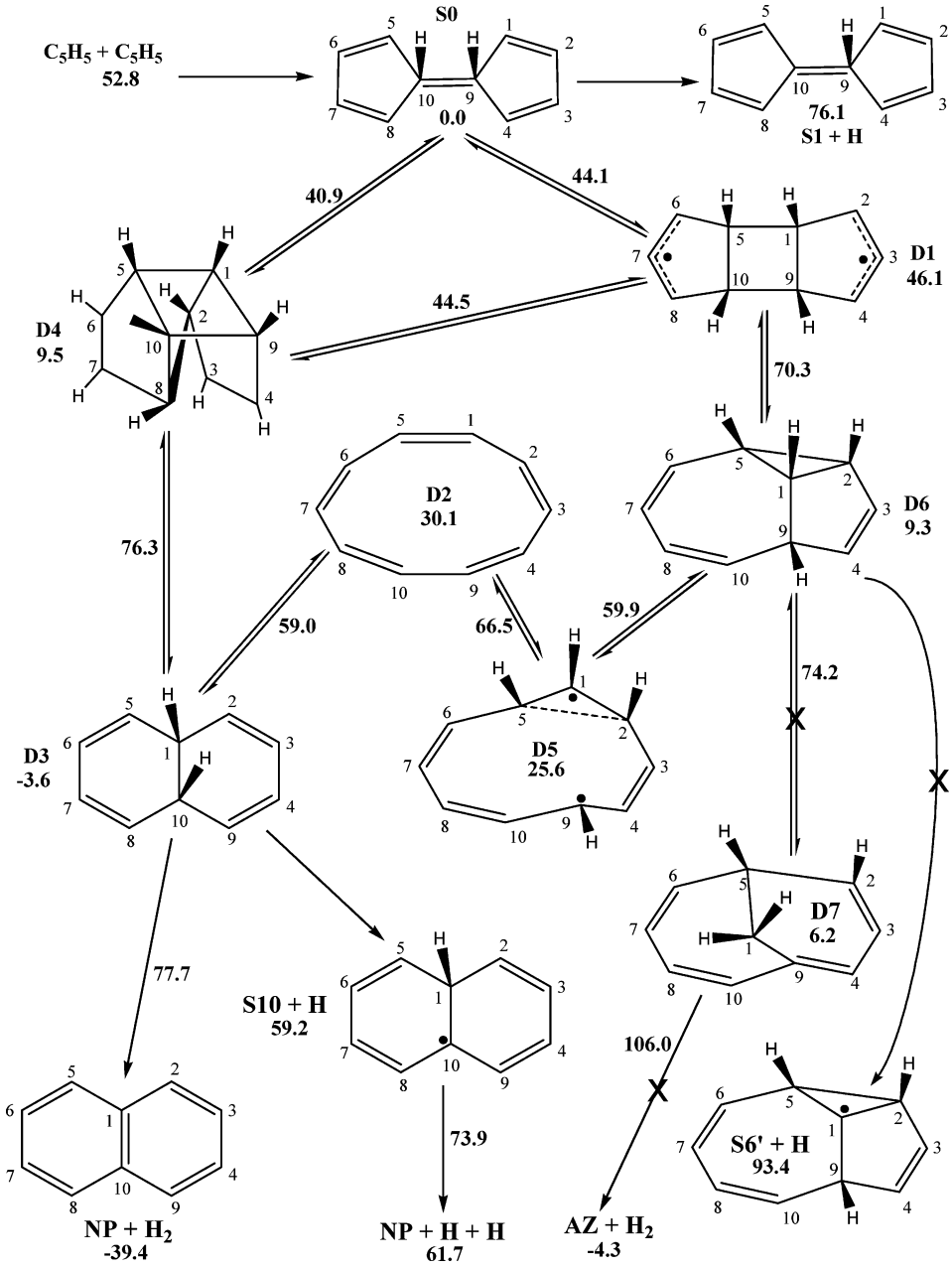

Figure 2. Potential energy map for the c-C_5H_5 + c-C_5H_5 → $C_{10}H_{10}$ → $C_{10}H_9$ + H/$C_{10}H_8$ + H_2 reaction. All relative energies are calculated at the G3(MP2,CC) level of theory and given in kcal/mol. Schematic structures of various intermediates with atomic numbering are also shown.

not exceeding 0.01−0.03 Å. TS S0-D4 is an exception, where the differences in CASSCF and B3LYP C−C distances for the newly forming C−C bonds reach 0.09 Å resulting in larger discrepancies between the CASPT2 and CCSD(T) single-point relative energies of up to ∼10 kcal/mol. Hereafter, we chose to rely on CCSD(T) results obtained either with CASSCF or B3LYP optimized structures, whichever gives the lowest single-point CCSD(T) energy. These CCSD(T) energies were then utilized for G3(MP2,CC) calculations and the G3(MP2,CC) relative energies are used for further discussion and RRKM calculations of the rate constants. However, it should be noted that the aforementioned differences between CASPT2 and CCSD(T) relative energies for **D2**, **D4**, **D6**, and TS S0-D4 appeared not to affect significantly our kinetics calculations of the total rate constants and product branching ratios because the reaction bottleneck corresponds to the **D1** → **D6** step.

Now we turn our attention to the diradical mechanism leading from the initial 9,10-dihydrofulvalene adduct **S0** to 9,10-dihydronaphthalene **D3** via the diradical intermediate **D1**. **S0** can be produced from the recombination of two cyclopentadienyl radicals in *cis*- and *trans*-conformations with the energy gain of 52.8 and 52.6 kcal/mol,[20] respectively. The barrier between the two is merely ∼5 kcal/mol,[20] and hereafter, we only consider the *cis*-9,10-dihydrofulvalene conformer. As seen in Figure 2, two reaction routes from **S0** to **D3** travel through **D1**, and we first consider the channel, which also involves **D2**. At the initial step, a C−C bond can be formed between carbon atoms 1 and 5 or 4 and 8 from two different five-member rings, producing a new four-member ring in the central part of **D1**. The barrier at the corresponding TS S0-D1 is calculated to be 44.1 kcal/mol. Geometry optimization and vibrational frequency calculations for **D1** show that it has a C_{2v}-symmetric structure and is a local minimum on the PES with all real frequencies, at least at the CASSCF level. However, all higher-level calculations, including CASPT2, CCSD(T), and G3(MP2,CC), gave the energy of **D1** slightly higher than those of the adjacent

transition states TS S0-D1 and TS D1-D4. This result indicates that the diradical **D1** is a metastable intermediate at best. While one cannot exclude that a higher energy geometry optimization (for example, at the CASPT2 level) would decrease the **D1** energy below those for the transition states, it is not likely that the barriers separating **D1** from **S0** or **D4** are significant. Next, the 1−9 and 5−10 bonds in **D1** can be cleaved to bring about the 10-member ring structure **D2**. However, a TS search followed by intrinsic reaction coordinate (IRC) calculations verifying connections of the found TSs to corresponding local minima shows that the **D1** → **D2** isomerization is a three-step process involving two intermediates, **D6** and **D5**. First, the 5−10 C−C bond breaks in **D1** to form a seven-member ring, but this is compensated by simultaneous formation of a new 2−5 bond and, thus, a tricyclic **D6** structure with the seven-member ring is produced. This rearrangement can occur by four different symmetric ways, only one of them is mentioned above. The relative energies of TS D1-D6 and **D6** are 70.3 and 9.3 kcal/mol, respectively. At the second step, the 1−9 bond breaks in **D6** and the 2−5 bond significantly elongates giving the second intermediate **D5**, which essentially has a strongly puckered 10-member ring geometry. The barrier for this step is 50.6 (59.9) kcal/mol relative to **D6** (**S0**) and **D5** resides 25.6 kcal/mol higher in energy than the initial **S0** adduct. Finally, **D5** rearranges to the 10-member ring structure **D2** (30.1 kcal/mol relative to **S0**) via a TS D2-D5 (66.5 kcal/mol). **D2** exhibits a boat configuration with very clearly expressed alteration of single (1.48 Å) and double (1.34 Å) C−C bonds. This intermediate further isomerizes to dihydronaphthalene **D3** made of two fused six-member rings by a C−C bond formation across the ten-member ring (for example, 1−10, 5−9, etc., a total of five different nearly symmetric possibilities, assuming that "breathing" conformational changes in the ring of **D2** are facile). The barrier at TS D2-D3 is 59.0 kcal/mol and **D3** is −3.6 kcal/mol relative to the initial adduct.

The alternative pathway from **S0** to **D3** proceeds via the intermediate **D4**, which has a C_2-symmetric structure with a nonplanar four-member ring in the middle, fused with two peripheral five-member rings connected to each other by a C−C bond (Figure 2). Going from **S0** to **D4**, two C−C bonds are created, between carbon atoms 1 and 5 as well as 2 and 8. The C_2 symmetry axis goes via the centers of the 2−8 bond and the 1−5−9−10 diamond. The barrier at TS S0-D4, 40.9 kcal/mol, is slightly lower than that at TS S0-D1. **D4** can be also easily produced from the metastable diradical structure **D1** by a C−C bond formation between the radical sites 2 and 8 or 4 and 6. The **D4** → **D3** isomerization at the next reaction step involves the formation of the 1−10 bond in the diagonal of the central diamond and the cleavage of the 5−10 and 1−9 bonds in this diamond as well as of the 2−8 bond. Meanwhile, the 2−3, 4−9, 5−6, and 7−8 C−C bonds acquire a double-bond character. This rather complicated process proceeds via a high barrier, with the transition state TS D4-D3, 76.3 kcal/mol above **S0**, having the highest energy among all TSs considered so far. Compared to the two-step **S0** → **D4** → **D3** route, the multistep **S0** → **D1** → **D6** → **D5** → **D3** pathway exhibits a lower critical barrier, 70.3 kcal/mol at TS D1-D6.

The dihydronaphthalene intermediate **D3** can decompose via two different paths. Elimination of an H atom produces the 9-H-naphthyl radical **S10** without an exit (reverse) barrier; the breaking C−H bond strength in **D3** is calculated to be 62.8 kcal/mol. Alternatively, molecular hydrogen loss from **D3** is highly exothermic but has to go via a large barrier of 81.3 (77.7) kcal/mol relative to **D3** (**S0**). Unimolecular decomposition of the **D6** intermediate is not expected to be competitive with its isomerization to **D5**. Although **D6** can lose an H atom to form the $C_{10}H_9$ structure **S6′** without an exit barrier, **S6′** + H lie 93.4 kcal/mol higher in energy than the initial adduct. Otherwise, **D6** can undergo a 1,2-H shift to **D7** followed by H_2 elimination producing azulene. However, the barriers at TS D6-D7 and TS D7-H_2, 74.2 and 106.0 kcal/mol with respect to **S0**, respectively, are too high for these channels to be viable. Even if **D7** can be produced, it represents a dead end on the PES because of very high energies required for H_2 or H eliminations and, therefore, the pathways from **D6** to **D7** and further were not included in our kinetic calculations.

TABLE 2: Product Branching Ratios Calculated at Different Temperatures[a]

T, K	**S1** + H	**S10** + H
300	0.1	99.9
500	17.8	82.3
600	45.9	54.1
700	70.3	29.7
800	83.2	16.8
900	90.2	9.8
1000	93.7	6.3
1100	95.6	4.4
1200	96.8	3.2
1300	97.6	2.5
1400	98.1	1.9
1500	98.4	1.6
1700	98.8	1.2
1900	99.1	0.9
2000	99.2	0.9
2200	99.3	0.8
2400	99.3	0.7
2600	99.4	0.6
2800	99.4	0.6
3000	99.5	0.6

[a] Calculated branching ratios of **NP** + H_2 do not exceed 10^{-3} %.

Now we can summarize potentially important reaction pathways, as follows:

S0 → **D1** → **D6** → **D5** → **D2** → **D3**
the highest barrier 70.3 kcal/mol

S0 → **D4** → **D3** or **S0** → **D1** → **D4** → **D3**
the highest barrier 76.3 kcal/mol

D3 → **NP** + H_2 the highest barrier 77.7 kcal/mol

D3 → **S10**(9-H-naphthyl) + H
endothermicity 59.2 kcal/mol

All these channels via **D3** to **S10** + H and **NP** + H_2 have to compete with the direct H loss from the initial 9,10-dihydrofulvalene adduct:

S0 → **S1**(9-H-fulvalenyl) + H
endothermicity 76.1 kcal/mol

RRKM calculations of rate constants in the subsequent section help us to shed light on this competition.

Product Branching Ratios and Thermal Rate Constants. Using RRKM rate constants for individual unimolecular reaction steps at the high-pressure limit shown in Table S2, we computed product branching ratios at different temperatures (Table 2).

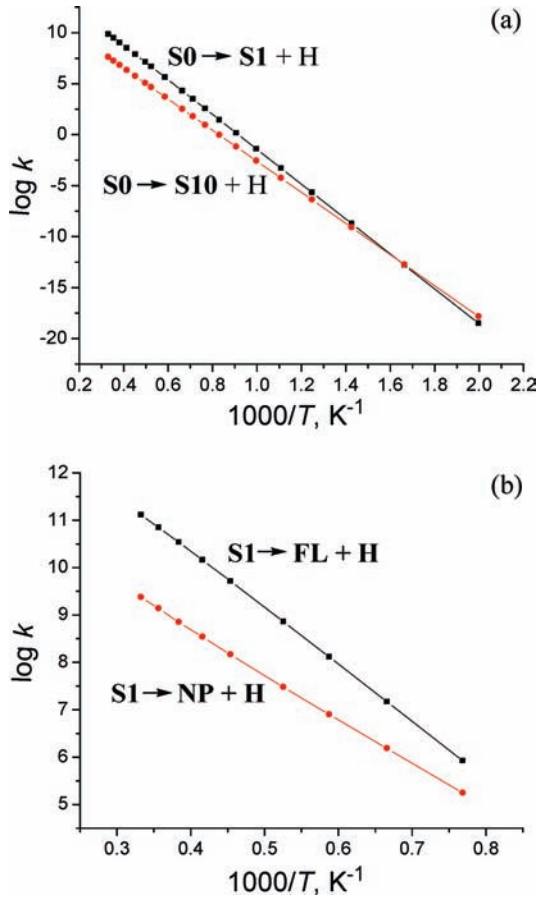

Figure 3. Calculated total high-pressure-limit thermal rate constants for the unimolecular decomposition reactions $C_{10}H_{10}$ (**S0**) → **S1** + H/**S10** + H (a) and $C_{10}H_9$ (**S1**) → **NP** + H/**FL** + H (b).

These calculations were performed by solving kinetic equations according to the reaction scheme shown in Figure 2 in the steady-state approximation. The results show that the **NP** + H_2 product channel is practically negligible at all temperatures considered. This owes to a high barrier at TS D3-H_2, which is 18.5 kcal/mol higher than the energy required for the H loss from **D3** and also to the fact that the H_2 elimination transition state is tight (i.e., it corresponds to a distinct barrier on the PES), on the contrary to loose variational transition states for splitting an H atom corresponding to a single C−H bond cleavage occurring without a reverse barrier. This makes the H_2 loss also entropically unfavorable. The H loss channel to produce 9-H-naphthyl **S10** has a higher relative yield than **S1** (9-H-fulvalenyl) + H at lower temperatures, up to ~600 K, but at higher temperatures, the **S1** + H products take over and become dominant at around 1000 K. Although the pathway to 9-H-naphthyl has a lower critical barrier of 70.3 kcal/mol compared to 76.1 kcal/mol required for the production of 9-H-fulvalenyl, this route is a multistep process proceeding via tight transition states and therefore it is disfavored by the entropy factor.

The implications of the computed branching ratios to combustion can be better understood if one considers absolute values of total rate constants for unimolecular decomposition of $C_{10}H_{10}$ **S0** to **S1** + H and **S10** + H (see Figure 3). The rate constants for the **S1** channel can be calculated directly because **S0** → **S1** + H is a one-step process, and to evaluate the **S0** → **S10** + H total rate constants we utilized the computed steady-state product branching ratios. In the temperature range of 300−600 K, where the **S1** + H products are preferable, the k(**S10** + H) rate constants have very low values, from 5.7×10^{-39} to 1.7×10^{-13} s^{-1}, that is, the reaction is expected to be too slow and insignificant. At higher temperatures, where the rates become faster, the 9-H-fulvalenyl product channel clearly dominates and the formation of 9-H-naphthyl on the $C_{10}H_{10}$ PES is predicted to be only minor. Three- and two-parameter fits of the rate constants in the 300−3000 K temperature range give the following expressions:

$$k(\mathbf{S0} \rightarrow \mathbf{S1} + \mathrm{H}) = 1.97 \times 10^{16} T^{-0.21} \exp(-78265/T)$$
$$3.71 \times 10^{15} \exp(-77919\ \mathrm{cal}/RT)$$

$$k(\mathbf{S0} \rightarrow \mathbf{S10} + \mathrm{H}) = 8.86 \times 10^{12} T^{-0.09} \exp(-69961/T)$$
$$4.41 \times 10^{12} \exp(-69812\ \mathrm{cal}/RT)$$

The two-parameter expressions describe the calculated rate constants fairly well and one can also see that the apparent activation energies, 77.9 and 69.8 kcal/mol for **S1** and **S10**, respectively, are close to the computed critical barriers on the respective reaction pathways, 76.1 and 70.3 kcal/mol. For combustion applications, it would be also important to derive rate expressions for the recombination of two cyclopentadienyl radicals followed by decomposition of chemically activated **S0**, that is, for the c-C_5H_5 + c-C_5H_5 → **S0** → **S1** + H /**S10** + H processes. This requires a careful consideration of the reaction path in the barrierless entrance channel and then the corresponding rate constants can be evaluated using CVTST or variable reaction coordinate (VRC)-TST.[35] Such work is currently underway in our group and will be reported in the future.

It is informative to compare the rate constants for unimolecular decomposition of 9,10-dihydrofulvalene **S0** ($C_{10}H_{10}$) with those for 9-H fulvalenyl **S1** ($C_{10}H_9$). A detailed analysis of the isomerization and dissociation pathways of **S1** and their individual thermal high-pressure limit rate constants have been published earlier.[20] Here, we used those rate constants to solve phenomenological kinetic differential equations and to compute concentrations of two leading decomposition products, fulvalene (**FL**) + H and naphthalene (**NP**) + H, as functions of time. These results were then utilized to derive the overall **S1** → **FL** + H and **S1** → **NP** + H rate constants at different temperatures. The computed values are plotted in Figure 3b and can be fitted by the following three- and two-parameter expressions (in s^{-1})

$$k(\mathbf{S1} \rightarrow \mathbf{FL} + \mathrm{H}) = 5.64 \times 10^{19} T^{-1.24} \exp(-59295/T)$$
$$1.28 \times 10^{15} \exp(-54534\ \mathrm{cal}/RT)$$

$$k(\mathbf{S1} \rightarrow \mathbf{NP} + \mathrm{H}) = 4.53 \times 10^{5} T^{1.83} \exp(-36345/T)$$
$$3.08 \times 10^{12} \exp(-43334\ \mathrm{cal}/RT)$$

For example, at 1500 K, the calculated values of k(**S1** → **FL** + H) and k(**S1** → **NP** + H) are 1.4×10^7 and 1.5×10^6 s^{-1}, respectively, compared to only 1.8×10^4 s^{-1} for **S0** → **S1** + H. The difference between the $C_{10}H_9$ and $C_{10}H_{10}$ decomposition rate constants remain significant even at 3000 K, where the computed values for **S1** → **FL** + H, **S1** → **NP** + H, and **S0** → **S1** + H, respectively, are 1.3×10^{11}, 2.3×10^9, and 6.5×10^9 s^{-1}. However, this difference should not be overstated because the reactions follow each other rather than being competitive and the dissociation of **S0** will be enhanced by chemical activation from the recombination of two c-C_5H_5.

4. Conclusions

Ab initio calculations of the $C_{10}H_{10}$ potential energy surface related to the reaction of two cyclopentadienyl radicals and some isomerization and dissociation pathways of their recombination product 9,10-dihydrofulvalene **S0** combined with RRKM calculations of thermal rate constants and product branching ratios at the high pressure limit show that at temperatures relevant to combustion the 9-H-fulvalenyl radical **S1** is expected to be the dominant reaction product. A naphthalene precursor, 9,10-dihydronaphthalene **D3**, can be formed from the initial adduct **S0** by a multistep diradical mechanism involving the formation of a metastable tricyclic diradical intermediate **D1**, followed by its eventual (three-step) opening to a 10-member ring structure **D2** and ring contraction in the latter producing the naphthalene core in **D3**. The highest barrier on the **S0** → **D3** pathway is calculated to be 70.3 kcal/mol. **D3** can lose molecular hydrogen producing naphthalene via a barrier of 77.7 kcal/mol (relative to **S0**) or a hydrogen atom giving rise to the 9-H-naphthyl radical **S10** without exit barrier and with overall endothermcity of 59.2 kcal/mol. The **S0** → **S10** + H multistep mechanism appears to be preferable as compared to the direct H atom elimination **S0** → **S1** + H at low temperatures (below 600 K), but the rate constants at these temperatures are too slow for the reaction to be significant. The **S0** → **NP** + H_2 multistep channel should not be viable at any temperature. Hypothetically, it is possible that **NP** + H_2 might be formed from 9,10-dihydronaphthalene **D3** by a roaming mechanism,[36] in which an H atom first leaves the molecule, then roams around and picks up the second hydrogen thus forming H_2. However, in this particular case, the roaming mechanism is not expected to be important because at the temperatures relevant to combustion **D3** would not be formed in the first place. Summarizing, the following reaction sequence can be suggested for kinetic models to take into account for the recombination of two cyclopentadienyl radicals

$$\text{c-}C_5H_5 + \text{c-}C_5H_5 \rightarrow \text{9,10-dihydrofulvalene} \rightarrow \text{9-H-fulvalenyl} + H(C_{10}H_{10}\text{PES})$$

$$\text{9-H-fulvalenyl} \rightarrow \text{naphthalene} + \text{H/fulvalene} + H(C_{10}H_9\text{PES})$$

Naphthalene can be produced from the recombination of two cyclopentadienyl radicals and is expected to be a favorable product of this reaction sequence at $T < 1000$ K, but this molecule would be formed through isomerizations and H atom loss on the $C_{10}H_9$ PES (after the initial H elimination from $C_{10}H_{10}$ **S0**) and not in conjunction with molecular hydrogen.

Acknowledgment. This work is funded by the Chemical Sciences, Geosciences and Biosciences Division, Office of Basic Energy Sciences, Office of Sciences of U.S. Department of Energy (Grant No. DE-FG02-04ER15570).

Supporting Information Available: Optimized Cartesian coordinates, total energies at the CASSCF/6-311G** and B3LYP/6-311G** levels of theory, zero-point energy corrections, moments of inertia, rotational constants, and vibrational frequencies of all species involved in the studied mechanisms (Table S1); RRKM calculated high-pressure limit thermal rate constants for all studied reactions within 300−3000 K temperature range (Table S2). This material is available free of charge via the Internet at http://pubs.acs.org.

References and Notes

(1) Melius, C. F.; Colvin, M. E.; Marinov, N. M.; Pitz, W. J.; Senkan, S. M. *Proc. Int. Symp. Combust.* **1996**, *26*, 685.
(2) Castaldi, M. J.; Marinov, N. M.; Melius, C. F.; Huang, J.; Senkan, S. M.; Pitz, W. J.; Westbrook, C. K. *Proc. Int. Symp. Combust.* **1996**, *26*, 693.
(3) Marinov, N. M.; Pitz, W. J.; Westbrook, C. K.; Vincitore, A. M.; Castaldi, M. J.; Senkan, S. M.; Melius, C. F. *Combust. Flame* **1998**, *114*, 192.
(4) Richter, H.; Howard, J. B. *Prog. Energy Combust. Sci.* **2000**, *26*, 565.
(5) Lindstedt, P.; Maurice, L.; Meyer, M. *Faraday Discuss.* **2001**, *119*, 409.
(6) Hansen, N.; Klippenstein, S. J.; Miller, J. A.; Wang, J.; Cool, T. A.; Law, M. E.; Westmoreland, P. R.; Kasper, T.; Kohse-Hoinghaus, K. *J. Phys. Chem. A* **2006**, *110*, 4376.
(7) Frenklach, M.; Wang, H. *Proc. Combust. Inst.* **1991**, *23*, 1559.
(8) Wang, D.; Violi, A.; Kim, D. H.; Mullholland, J. A. *J. Phys. Chem. A* **2006**, *110*, 4719.
(9) Colussi, A. J.; Zabel, F.; Benson, S. W. *Int. J. Chem. Kinet.* **1977**, *9*, 161.
(10) Lin, C.-Y.; Lin, M. C. *Int. J. Chem. Kinet.* **1985**, *17*, 1025; *J. Phys. Chem.* **1986**, *90*, 425.
(11) Carpenter, B. K. *J. Am. Chem. Soc.* **1993**, *115*, 5−9806; *J. Phys. Chem.* **1995**, *99*, 9801.
(12) Olivella, S.; Sole, A.; Garcia-Raso, A. *J. Phys. Chem.* **1995**, *99*, 10549.
(13) Liu, R.; Morokuma, K.; Mebel, A. M.; Lin, M. C. *J. Phys. Chem.* **1996**, *100*, 9314.
(14) Fadden, M. J.; Barckholtz, C.; Hadad, C. M. *J. Phys. Chem. A* **2000**, *104*, 3004.
(15) Tokmakov, I. V.; Kim, G.-S.; Kislov, V. V.; Mebel, A. M.; Lin, M. C. *J. Phys. Chem. A* **2005**, *109*, 6114.
(16) Moskaleva, L. V.; Lin, M. C. *J. Comput. Chem.* **2000**, *21*, 415.
(17) Moskaleva, L. V.; Mebel, A. M.; Lin, M. C. *Proc. Int. Symp. Combust.* **1996**, *26*, 521.
(18) (a) Fascella, S.; Cavallotti, C.; Rota, R.; Carra, S. *J. Phys. Chem. A* **2005**, *109*, 7546. (b) Cavallotti, C.; Mancarella, S.; Rota, R.; Carra, S. *J. Phys. Chem. A* **2007**, *111*, 3959.
(19) Kislov, V. V.; Mebel, A. M. *J. Phys. Chem. A* **2008**, *112*, 700.
(20) Kislov, V. V.; Mebel, A. M. *J. Phys. Chem. A* **2007**, *111*, 9532.
(21) Dyakov, Y. A.; Ni, C.-K.; Lin, S. H.; Lee, Y. T.; Mebel, A. M. *J. Phys. Chem. A* **2005**, *109*, 8774.
(22) Carpenter, B. K. private communication.
(23) (a) Becke, A. D. *J. Chem. Phys.* **1992**, *96*, 2155. (b) Becke, A. D. *J. Chem. Phys.* **1992**, *97*, 9173. (c) Becke, A. D. *J. Chem. Phys.* **1993**, *98*, 5648. (d) Lee, C.; Yang, W.; Parr, R. G. *Phys. Rev. B: Condens. Matter Mater. Phys.* **1988**, *37*, 785.
(24) Jensen, H. J. Aa.; Ågren, H.; Olsen, J. Modern Techniques in Computational Chemistry. In *SIRIUS: a general-purpose direct second-order MCSCF program*; Clementi, E., Ed.; ESCOM: Leiden, 1991.
(25) Werner, H.-J. *Mol. Phys.* **1996**, *89*, 645.
(26) (a) Baboul, A. G.; Curtiss, L. A.; Redfern, P. C.; Raghavachari, K. *J. Chem. Phys.* **1999**, *110*, 7650. (b) Curtiss, L. A.; Raghavachari, K.; Redfern, P. C.; Baboul, A. G.; Pople, J. A. *Chem. Phys. Lett.* **1999**, *314*, 101.
(27) Curtiss, L. A.; Raghavachari, K.; Redfern, P. C.; Rassolov, V.; Pople, J. A. *J. Chem. Phys.* **1998**, *109*, 7764.
(28) Angeli, C.; Bak, K. L. ; Bakken, V.; Christiansen, O.; Cimiraglia, R.; Coriani, S.; Dahle, P.; Dalskov, E. K.; Enevoldsen, T.; Fernandez, B.; Hättig, C.; Hald, K.; Halkier, A.; Heiberg, H.; Helgaker, T.; Hettema, H.; Jensen, H. J. Aa.; Jonsson, D.; Jøgensen, P.; Kirpekar, S.; Klopper, W.; Kobayashi, R.; Koch, H.; Ligabue, A.; Lutnæs, O. B.; Mikkelsen, K. V.; Norman, P.; Olsen, J.; Packer, M. J.; Pedersen, T. B.; Rinkevicius, Z.; Rudberg, E.; Ruden, T. A.; Ruud, K.; Salek, P.; Sanchez de Meras, A.; Saue, T.; Sauer, S. P. A.; Schimmelpfennig, B.; Sylvester-Hvid, K. O.; Taylor, P. R.; Vahtras, O.; Wilson, D. J.; Ågren, H. *Dalton, a molecular electronic structure program*, Release 2.0; 2005, http://www.kjemi.uio.no/software/dalton/dalton.html.
(29) Frisch, M. J.; Trucks, G. W.; Schlegel, H. B.; Scuseria, G. E.; Robb, M. A.; Cheeseman, J. R.; Zakrzewski, V. G.; Montgomery, J. A.; Stratmann, R. E.; Burant, J. C.; Dapprich, S.; Millam, J. M.; Daniels, R. E.; Kudin, K. N.; Strain, M. C.; Farkas, O.; Tomasi, J.; Barone, V.; Cossi, M.; Cammi, R.; Mennucci, B.; Pomelli, C.; Adamo, C.; Clifford, S.; Ochterski, J.; Petersson, G. A.; Ayala, P. Y.; Cui, Q.; Morokuma, K.; Salvador, P.; Dannenberg, J. J.; Malick, D. K.; Rabuck, A. D.; Raghavachari, K.; Foresman, J. B.; Cioslowski, J.; Ortiz, J. V.; Baboul, A. G.; Stefanov, B. B.; Liu, G.; Liashenko, A.; Piskorz, P.; Komaromi, I.; Gomperts, R.; Martin, R. L.; Fox, D. J.; Keith, T.; Al-Laham, M. A.; Peng, C. Y.; Nanayakkara, A.; Challacombe, M.; Gill, P. M. W.; Johnson, B.; Chen, W.; Wong, M. W.; Andres, J. L.; Gonzalez, C.; M. Head-Gordon, M.; Replogle, E. S.; Pople, J. A. *Gaussian 98*, revision A.11; Gaussian, Inc.: Pittsburgh, PA, 2001.

(30) Amos, R. D.; Bernhardsson, A.; Berning, A.; Celani, P.; Cooper, D. L.; Deegan, M. J. O.; Dobbyn, A. J.; Eckert, F.; Hampel, C.; Hetzer, G.; Knowles, P. J.; Korona, T.; Lindh, R.; Lloyd, A. W.; McNicholas, S. J.; Manby, F. R.; Meyer, W.; Mura, M. E.; Nicklass, A.; Palmieri, P.; Pitzer, R.; Rauhut, G.; Schutz, M.; Schumann, U.; Stoll, H.; Stone, A. J.; Tarroni, R.; Thorsteinsson, T.; Werner, H.-J. *MOLPRO*, a package of ab initio programs designed by Werner, H.-J. and Knowles, P. J.; version 2006 1, 2006.

(31) (a) Steinfield, J.; Francisco, J.; Hase, W. *Chemical Kinetics and Dynamics*; Prentice-Hall: Englewood Cliffs, NJ, 1989. (b) Eyring, H.; Lin, S. H.; Lin, S. M. *Basic Chemical Kinetics*; Wiley: New York, 1980. (c) Robinson, P. J.; Holbrook, K. A. *Unimolecular Reactions*; Wiley: New York, 1972.

(32) (a) Wigner, E. *J. Chem. Phys.* **1937**, *5*, 720. (b) Truhlar, D. G.; Isaacson, A. D.; Garrett, B. C. In *Theory of Chemical Reaction Dynamics*; Baer, M., Ed.; CRC Press: Boca Raton, FL, 1985; Vol. 4, p 65. (c) Truhlar, D. G.; Garrett, B. C. *Annu. Rev. Phys. Chem.* **1984**, *35*, 159.

(33) Press, W. H.; Teukolsky, S. A.; Vetterling, W. T., Flannery, B. P. *Numerical Recipes in Fortran 77. The Art of Scientific Computing*, 2nd ed.; Cambridge University Press: Cambridge, 1992.

(34) (a) Lee, T. J.; Taylor, P. R. *Int. J. Quant. Chem. Symp.* **1989**, *23*, 199. (b) Cramer, C. J. *Essential of Computational Chemistry*; Wiley: Chichester, 2002, p 212.

(35) (a) Klippenstein, S. J. *Chem. Phys. Lett.* **1990**, *170*, 71. (b) Klippenstein, S. J. *J. Chem. Phys.* **1991**, *94*, 6469. (c) Klippenstein, S. J. *J. Chem. Phys.* **1992**, *96*, 367. (d) Robertson, S. H.; Wagner, A. F.; Wardlaw, D. M. *Faraday Disc. Chem. Soc.* **1995**, *102*, 65.

(36) Townsend, D.; Lahankar, S. A.; Lee, S. K.; Chambreau, S. D.; Suits, A. G.; Zhang, X.; Rheinecker, J.; Harding, L. B.; Bowman, J. M. *Science* **2004**, *306*, 1158.

JP905931J